Three-Dimensional Solution Structure of the Cyanide Adduct of a Met80Ala Variant of *Saccharomyces cerevisiae* Iso-1-cytochrome *c*. Identification of Ligand−Residue Interactions in the Distal Heme Cavity†

Lucia Banci,‡ Ivano Bertini,*,‡ Kara L. Bren,§ Harry B. Gray,*,§ Pornthep Sompornpisut,‡ and Paola Turano‡

Department of Chemistry, University of Florence, Via Gino Capponi 7, 50121, Florence, Italy, and Arthur Amos Noyes Laboratory, California Institute of Technology, Pasadena, California 91125

Received April 10, 1995; Revised Manuscript Received June 28, 1995®

ABSTRACT: The ^{1}H NMR spectrum of the the cyanide adduct of a triply mutated *Saccharomyces cerevisiae* iso-1-cytochrome *c* (His39Gln/Met80Ala/Cys102Ser) in the oxidized form has been assigned through 1D NOE and 2D COSY, TOCSY, NOESY, and NOE-NOESY experiments; 562 protons out of a total of 683 have been assigned. The solution structure, the first of a paramagnetic heme protein, was determined using 1426 meaningful NOE constraints out of a total of 1842 measured NOEs. The RMSD values at the stage of restrained energy minimization of 17 structures obtained from distance geometry calculations are 0.68 ± 0.11 and 1.32 ± 0.14 Å for the backbone and all heavy atoms, respectively. The quality, in terms of RMSD, of the present structure is the same as that obtained for the solution structure of the diamagnetic horse heart ferrocytochrome *c* [Qi, P. X., et al. (1994) *Biochemistry 33,* 6408−6419]. The secondary structure elements and the overall folding in the variant are observed to be the same as those of the wild-type protein for which the X-ray structure is available. However, the replacement of the methionine axial ligand with an alanine residue creates a ligand-binding "distal cavity." The properties of the distal cavity seen in this solution structure are compared to those of other heme proteins.

The transformation of a protein that performs a certain function into one with a different function is a key step in the understanding of the structure/function relationships. In the case of dioxygen-binding heme proteins, site-directed mutagenesis experiments have shown that the distal His (position E7) in the heme cavity of myoglobin plays a key role in stabilizing the Fe−O_2 complex by hydrogen bonding, while disfavoring Fe−CO bonding (Springer et al., 1989; Smerdon et al., 1991a,b; Rohlfs et al., 1990; Egeberg et al., 1990; Carver et al., 1992). It also appears that oxymyoglobin can be stabilized by the presence of an aromatic residue in the distal pocket, since the Leu29Phe mutant of sperm whale myoglobin exhibits an unusually high Fe−O_2 binding constant and low autoxidation rate (Carver et al., 1992). In addition, it is likely that a B-helix Phe is responsible for the stability of the Fe−O_2 unit in elephant myoglobin, where a Gln is present in the E7 position (Vyas et al., 1993). Recently an electron transfer protein, cytochrome *c*, (Moore & Pettigrew, 1990; Pettigrew & Moore, 1987) was transformed into a dioxygen-carrying molecule through site-directed mutagenesis (Lu et al., 1993). In particular, Met80, which is bound to the heme iron in wild-type cytochrome *c*, was substituted with an alanine to produce an iron center that is able to carry dioxygen in the reduced state. The dioxygen complex has a higher binding constant and a lower autoxidation rate than myoglobin (Bren & Gray, 1993; Lu et al., 1993).

By employing ^{1}H NMR spectroscopy, we have solved the three-dimensional solution structure of the cyanide derivative of a triply mutated oxidized *Saccharomyces cerevisiae* iso-1-cytochrome *c* (His39Gln/Met80Ala/Cys102Ser) (MW 12 600), which is here referred to as Ala80cyt *c* in order to underline the mutation at the iron coordination site. The cyanide moiety may simulate the dioxygen molecule, and the structure shows the interactions of cyanide within the cavity. The cyanide−ferri form represents a challenge because, while the solution structures of three reduced diamagnetic cytochromes have been reported (Qi et al., 1994; Detlefsen et al., 1991; Blackledge et al., 1995), the present structure is the first of a paramagnetic cytochrome.

Cyanide derivatives of ferriheme-containing proteins may be suitable for NMR investigation in that the contribution to nuclear relaxation due to the hyperfine coupling with the single unpaired electron of low-spin iron(III) may be relatively small (Bertini & Luchinat, 1986; Bertini et al., 1993; Banci et al., 1991a). This holds for the oxidized proteins myoglobin [Emerson & La Mar (1990), and references therein] and several peroxidases (La Mar et al., 1995; Sette et al., 1993, and references therein) (Ferrer et al., 1994; Banci et al., 1991b,c, 1992, 1993b; Satterlee et al., 1990, 1991; Satterlee & Erman, 1980, 1991; Thanabal & La Mar, 1989; de Ropp et al., 1991), whereas in the cyanide adduct of cytochrome P450 the above coupling causes sizable proton line broadening (Banci et al., 1993a). We have already reported an investigation of the hyperfine shifted signals of the cyanide derivative of Ala80cyt *c* (Bren et al., 1995). We report here the solution structure of the entire protein. The steric properties of the distal cavity and the cyanide−residue interactions, as observed in this solution structure, are related to the mutant's dioxygen-binding properties.

† The structure coordinates have been deposited in the Brookhaven Protein Data Bank (file name 1FHB).

‡ University of Florence.

§ California Institute of Technology.

® Abstract published in *Advance ACS Abstracts,* August 15, 1995.

0006-2960/95/0434-11385$09.00/0

MATERIALS AND METHODS

Sample Preparation. Ala80cyt *c*, with mutations at positions 39 (His39Gln), 80 (Met80Ala) and 102 (Cys102Ser), was expressed and purified as previously reported (Lu et al., 1993). Owing to the low yield, no attempts were made to use stable isotope-labeling techniques. The ^{1}H NMR samples (in H_2O and in D_2O) were prepared by dissolving the lyophilized protein in 50 mM phosphate buffer at pH 7 to give 3 mM solutions. The pH of protein samples prepared for NMR spectroscopy was adjusted by addition of small volumes of concentrated solutions of NaOH and H_3PO_4. The pH was measured (uncorrected for the isotope effect) with an Orion Model 720 pH meter and a Microelectrodes, Inc. Model MI-410 microcombination pH probe.

NMR Spectroscopy. The ^{1}H NMR spectra were recorded on a Bruker MSL 200 (operating at 200.13 MHz) or an AMX 600 (operating at 600.13 MHz) spectrometer. The 200 MHz ^{1}H NMR 1D spectra were recorded using a superWEFT (water-eliminated Fourier transform) (Inubushi & Becker, 1983) pulse sequence with recycle delay of 200−250 ms. The 600 MHz ^{1}H NMR 1D spectra were obtained using presaturation during relaxation delay (550−800 ms), to eliminate the water signal. The ^{1}H nuclear Overhauser effect (NOE) experiments (at 200 and 600 MHz) were performed with the superWEFT pulse sequence for water signal suppression and were collected using the previous reported methodology (Unger et al., 1985; Banci et al., 1989). Difference spectra were collected by applying the decoupler frequency on- and off-resonance, alternately, according to the scheme ω, $\omega + \delta$, ω, $\omega - \delta$.

TPPI NOESY (Macura et al., 1982; Marion & Wüthrich, 1983) and TOCSY (Bax & Davis, 1985) spectra were recorded with presaturation of the solvent signal both during the relaxation delay and the mixing time. To optimize the detection of cross peaks involving fast-relaxing resonances, NOESY and TOCSY maps at 295 and 303 K in D_2O solution (90% D_2O/10% H_2O) were recorded on the full spectral width (59.5 ppm) with recycle time of 550 ms and mixing time of 15 ms for NOESY and spin lock of 18 ms for TOCSY. To optimize the detection of connectivities in the diamagnetic region, NOESY and cleanTOCSY (Griesinger et al., 1988) maps in D_2O and H_2O (90% H_2O/10% D_2O) solutions were recorded on a smaller spectral width (30 ppm) with a recycle time of 800 ms and mixing times of 25 and 100 ms for NOESY and spin lock times of 30, 60, and 90 ms for TOCSY. A trim pulse was applied before the mixing time. A magnitude COSY (Bax et al., 1981; Bax & Freeman, 1981) map was recorded in H_2O solution on a 30 ppm spectral width (recycle time 800 ms). A NOE-NOESY experiment (Bertini et al., 1994) with a mixing time of 70 ms was performed by using the conventional NOESY sequence preceded by (180° pulse) − (τ delay) to select relatively fast relaxing resonances. During the τ delay (200 ms), a selective irradiation of the 5-CH_3 signal was performed. Analogously to the 1D NOE experiments, a difference map was collected by applying the decoupler frequency on- and off-resonance, alternately, during the τ delay and alternating accordingly the phase of the receiver.

All 2D spectra consisted of 4K data points in the *F*2 dimension. From 800 to 1024 experiments were recorded in the *F*1 dimension, using 64−192 scans/experiment. Raw data were multiplied in both dimensions by a pure cosine-squared (NOESY, TOCSY, NOE-NOESY) and a pure sine-squared (COSY) bell window function and Fourier-transformed to obtain 2048 × 2048 real data points. A polynomial baseline correction was applied in both directions. The spectra were calibrated by assuming a chemical shift of 4.85 and 4.75 ppm for the water signal with respect to 2,2-dimethyl-2-silapentane-5-sulfonate (DSS) at 295 and 303 K, respectively.

Data processing was performed by using a standard Bruker software package. The 2D maps were analyzed on IBM RISC 6000 computers with the program XEASY (ETH, Zürich) (Eccles et al., 1991).

Distance Geometry Calculations. The volumes of the cross peaks between assigned resonances were obtained using the integration routines present in the program XEASY. Most of the dipolar connectivities were taken from the 100 ms NOESY in H_2O solution at 303 K. Connectivities whose volumes could be better measured in other spectra recorded with the same parameters, but either at a different temperature or in D_2O solution, were scaled by referring to a few intraresidue connectivities whose volumes could be accurately measured in both spectra.

NOESY cross-peak intensities were converted into upper limits of interatomic distances by use of the program CALIBA (Güntert et al., 1991). As previously described by Wüthrich et al. (Wüthrich, 1989; Güntert et al., 1991; Eccles et al., 1991; Güntert & Wüthrich, 1991), the upper limits obtained from CALIBA were classified as (i) intraresidue except NH, Hα, and Hβ; (ii) sequential and intraresidue NH, Hα, and Hβ; (iii) medium-range (all nonsequential interresidue connectivities between NH, Hα, and Hβ within a segment of five consecutive residues); (iv) long-range backbone; and (v) long range. For NOEs involving methyl groups, the upper limits were evaluated independently using five analogous classes. The experimental distance constraints were then used to generate protein conformers by using the distance geometry (DG) program DIANA (Güntert et al., 1991).

Upper and lower distance limits were imposed to build up the heme (see Results for details). In addition, the nonstandard amino acid trimethyllysine present in position 72 was built and added to the DIANA library.

With the preliminary structures available, the scaling factors for the volume-to-distance conversion for each class were evaluated by plotting volumes of peaks arising from pairs of protons at fixed distance. As the structure emerged from successive runs of DG calculation, selected interatomic distances were taken from these structures and additional calibrations were performed. Several cycles of the structure calculation were carried out in order to recalibrate the NOE distance constraints; new NOESY cross peaks could now be assigned using the program ASNO (Güntert et al., 1993).

For the DG calculations, the default minimization parameters were used with the following exceptions: the maximal number of target function evaluations was increased to 3000 at all levels except the final three, where a number of 7000 proved to yield an optimal convergence for the calculated structures. In addition to the standard procedure of the distance geometry calculations, extensive use of the redundant angle strategy (REDAC) (Güntert & Wüthrich, 1991) was employed for the definition of starting conformations. Angle constraints for dihedral angles were only accepted by the program if in at least 10 structures the local target function for the residue in question was equal to or smaller than 0.4 Å^2, while during the last four REDAC cycles the

target function per residue cutoff criterion was 0.1 Å^2 to exclude the meaningless angle constraints. The final distance geometry calculation on 39 structures was performed without angle constraints to prove convergence. The program GLOMSA (Güntert et al., 1991) yielded 60 stereospecific assignments for diastereotopic protons.

Restrained Energy Minimization and Restrained Molecular Dynamics. Restrained energy minimization (REM) and restrained molecular dynamics (RMD) calculations on the family of 17 structures obtained from DG calculations, with the lowest target function, were performed with the SANDER module of the AMBER 4.0 program package (Pearlman et al., 1991). The force field parameters for all of the residues, except for the heme, the two iron axial ligands, and the heme-bound cysteines, were the standard AMBER "all atom" parameters (Weiner et al., 1986). The topology file for the heme was adapted from that of a heme *b*, available in the 4.0 release of AMBER and modified in order to take into account the structure of heme *c*. In particular, the two vinyl groups of heme *b* were modified to $CHCH_3$ moieties. The heme-bound cysteines, Cys14 and Cys17, were obtained from the normal cysteines by removing the terminal hydrogen and then linking the α-carbon of the 2-thioether and of the 4-thioether, respectively, of the heme to the cysteine sulfur atom with a covalent bond. The force constants for this bond (stretching, bending, torsion) were taken as those used for the sulfur and the CH_3 group of a methionine. The force field parameters, except for the charges, for the heme moiety and for the axial histidine were taken from the standard AMBER database, when available. Alternatively, they were taken to be equal to those already used for MD calculations on peroxidases (Banci et al., 1994), which were derived from data obtained on porphyrin model complexes (Argos & Mathews, 1975; Ruf et al., 1979; Dawson et al., 1982; Case & Karplus, 1979; Angelucci et al., 1993). The parameters for the cyanide and for its bond with the iron were derived from data obtained on small metal−cyanide complexes (Nakamoto et al., 1971; Jones, 1971; Nakamoto, 1978; Hancock, 1989). The charges of the iron, the heme (including the thioethers), the cyanide, and the axial histidine were determined through semiempirical calculations, using the MOPAC 5.0 program (F. J. Seiler Research Laboratory, U.S. Air Force Academy, Colorado Springs, CO). The AM1 Hamiltonian was used for the SCF calculations. The charges of equivalent atoms in the porphyrin ring were taken as the average of the calculated charges (the difference never being larger than 10% of each point charge). The nonstandard amino acid trimethyllysine was built with the PREP module of AMBER, and its charges were determined with the MOPAC 5.0 program.

Each structure of the DG family was energy minimized to a rms energy gradient lower than 0.4 kJ mol^{-1} Å^{-2} with the inclusion of the NOE- and H-bond-derived distance constraints (REM calculation). Then RMD calculations were performed on each structure. The calculations were performed for 48 ps, heating the system from 0 K to the equilibrium temperature of 300 K. The systems were coupled to a thermal bath at 300 K with a constant of 0.1 ps (Berendsen et al., 1984). The calculations were performed in vacuo, with a distance-dependent dielectric constant. The time step used was 1.5 fs; the bond lengths were kept fixed by the SHAKE algorithm (van Gunsteren & Berendsen, 1977) during the MD calculations, but not during the energy minimization. The nonbonded interactions were evaluated

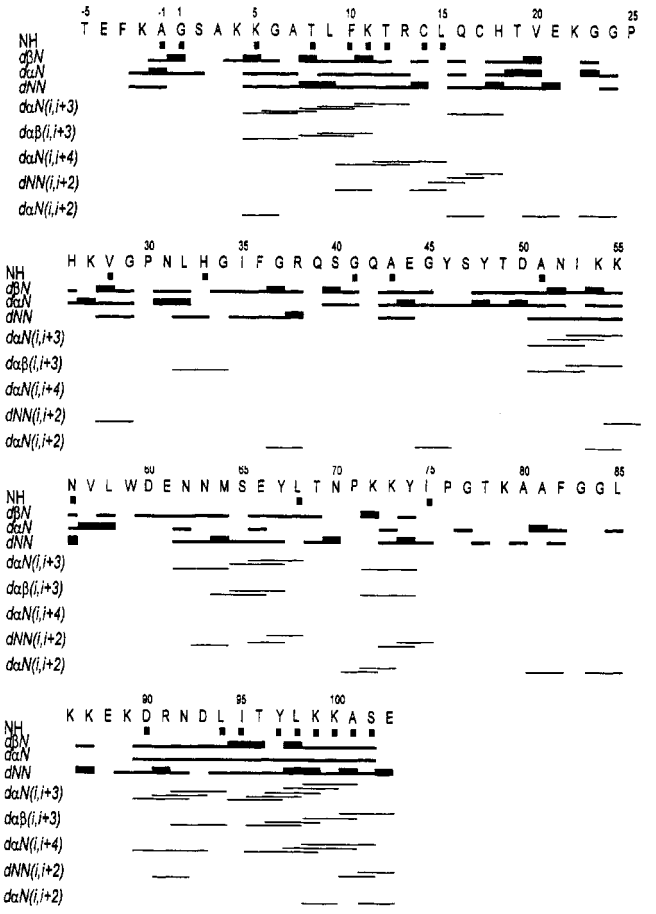

FIGURE 1: Schematic representation of the sequential connectivities involving NH, Hα, and Hβ protons in the cyanide adduct of Ala80cyt *c*. For the sequential connectivities, the thickness of the bar indicates the NOE intensities. The medium-range NOEs are identified by lines connecting the two correlated residues. In the first line, NH resonances that have been found to exchange slowly in D_2O solution are also indicated.

with a cutoff of 10 Å, and the pair list for the evaluation of the nonbonded interactions was updated every 20 steps. During the REM and the RMD calculations, the NOE-derived distance contraints were applied through the mixed linear-harmonic potential used by the SANDER module. The harmonic force constant was set to 134 kJ mol^{-1} Å^{-2}. The upper limit distances used by DIANA were taken as the upper limit for the application of the harmonic potential.

The final 24 ps of the RMD trajectory for each structure of the family was used to generate average structures with the CARNAL program (Ross, 1994). These average structures were then restrained energy minimized.

The DG, REM, and RMD calculations (double-precision accuracy) were performed on IBM RISC 6000 computers.

Structure Analysis. The structure analysis in terms of Ramachandran plots, deviation from ideal structural parameters, secondary structure elements, etc., was performed with the PROCHECK program (Laskowski et al., 1993). Visual inspection and drawings of the various families were performed with the programs SYBYL (Tripos Associates Inc.) and RASMOL (Sayle, 1994).

RESULTS

Sequence-Specific Assignment

Backbone Sequence-Specific Assignment. Sequential stretches for amide−amide proton connectivities obtained

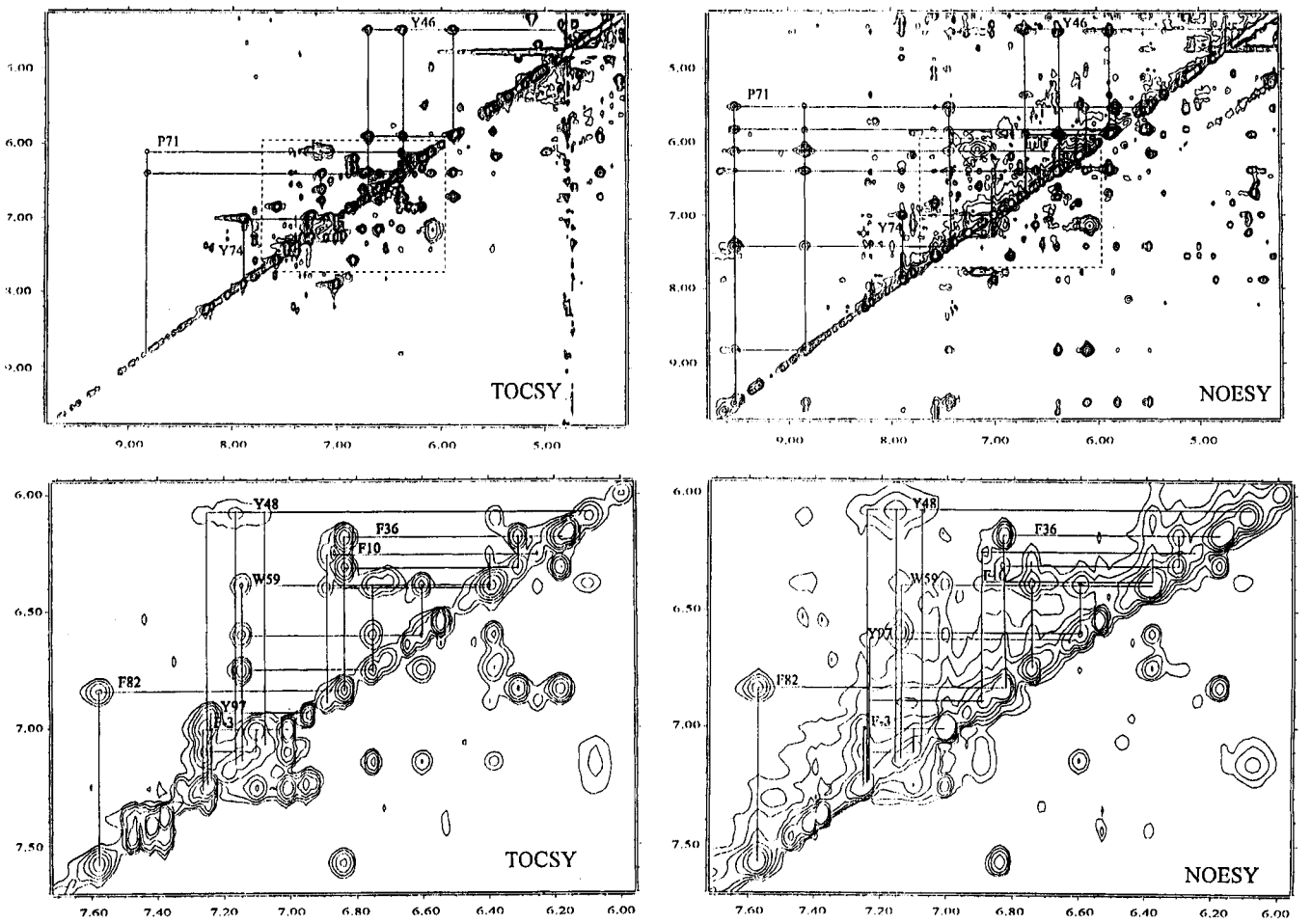

FIGURE 2: TOCSY [panels A (top left) and C (bottom left)] and intraresidue NOESY [panels B (top right) and D (bottom right)] connectivities observed for the ring protons of the aromatic residues and for the protons of Pro71. The TOCSY map was recorded with a spin lock time of 90 ms and the NOESY map with a 100 ms mixing time. Both spectra were recorded at 600 MHz in D_2O solution (50 mM phosphate buffer pH 7.0, 303 K).

from NOESY spectra (mixing times 25 and 100 ms) recorded in water are shown in Figure 1. Lower values of temperature cause a decrease of the NH proton exchange rate and, therefore, favor the detection of the connectivities in which the NH protons are involved. Sequential NH−NH connectivities for stretches longer than two residues were observed for positions −3 to −1, 4−14, 15−21, 27−29, 31−33, 36−38, 50−56, 61−67, 68−70, 72−75, 88−92, and 93 to the C-terminus. Sequential connectivities have not been observed for the entire protein chain due to the presence of four prolines (Pro25, Pro30, Pro71, Pro76) which do not contain the amide NH. Possible NH−NH connectivities at positions 14, 26, 38, 41, 56, 67, 87, and 92 cannot be observed because of nearly degenerate amide proton chemical shifts at positions i and $i + 1$. Connectivities involving the NH of residues −5, −4, 3, 59, and 84 are unobservable because the corresponding resonances have not been located. All other amide protons have been assigned and the NOEs expected on the basis of the final structure observed, with three exceptions. The distance between the amide protons of residues 1 and 2 and 43 and 44 is ~3.4 Å; however, the corresponding connectivities are expected at the same position of NH−NH connectivities between residues 62 and 63 and between residues 98 and 99, respectively. The latter two cross peaks are much more intense as they correspond to shorter distances (~2.6−2.7 Å) and therefore make difficult the observation of the former cross peaks. The expected connectivity between residues 44 and 45 has not been detected. This can be explained in terms of severe reduction of intensity of the corresponding NH resonances. In accordance with this hypothesis, the corresponding intraresidue NH−Hα cross peaks also have reduced intensity, although they are still detectable. Comparative analysis of the dipolar and scalar connectivities observed in the fingerprint region of the 2D NOESY and COSY experiments allowed us to obtain the complete sequence specific assignment for the backbone protons of 98 amino acids (Figure 1). TOCSY spectra were then used to obtain Hβ and Hγ assignments from the NH protons for several residues.

Relevant Residue Assignments. Comparison of the backbone sequence-specific assignments with the spin patterns, obtained from the analysis of the TOCSY maps, has led to the sequence-specific assignments available as Supporting Information. The results correspond to the assignment of 82% of the protons, of which 94% are for the backbone and 77% are for the side chains. Only the first two residues in the N-terminus (i.e., Thr-5 and Glu-4) remain completely unidentified. All assignments were obtained by using the standard procedure (Wüthrich, 1986). Here, we concentrate our discussion on the assignment of a few residues that we believe to be particularly relevant. An enlargment of the aromatic region of NOESY and TOCSY maps is shown in Figure 2. The pattern of Trp59 (the only Trp present in the sequence) is clearly evident. The Tyr67 spin system is better identified in the TOCSY map recorded with a spin lock time of 30 ms (Brem et al., 1995). This can be easily explained

on the basis of the vicinity of this aromatic ring to the paramagnetic center and therefore of the paramagnetic effect on the T_1 and T_2 values of its resonances. The assignment of this residue has never been reported in the up-to-date published assignments of different ferricytochromes *c*. The inability to detect this group in other cytochromes *c* was attributed to the flipping of the Tyr67 ring at a rate that is intermediate on the NMR chemical shift time scale (Qi et al., 1994; Wand et al., 1989; Moore & Williams, 1980a,b) which is not the case in the present system. The analysis of the aromatic side-chain assignments of the Tyr and Phe residues gives information on the mobility of these rings. As reported for the C102T protein (Gao et al., 1990), the observation of only one δ/ϵ scalar connectivity for Phe-3, Phe36, and Tyr74 (Figure 2A,C) indicates that their rings are flipping rapidly. For Phe82, only two resonances were detected for all the investigated temperatures. The assignment of the ring protons is based on the NOESY connectivities observed from these resonances. A similar situation was reported for the Phe82 ring in C102T yeast iso-1-ferricytochrome *c* without bound cyanide (Gao et al., 1990), where the Phe82 ring was considered to be flipping rapidly. For the present variant the same behavior may be suggested. On the other hand, Phe10, Tyr46, Tyr48, Tyr67, and Tyr97 are flipping slowly, as indicated by the observation of more than one set of δ/ϵ connectivities. Slow flipping for these residues, except for Tyr67 (see above), is consistent with the literature data on other cytochromes (Qi et al., 1994; Wand et al., 1989; Moore & Williams, 1980a,b). In the aromatic region, the spin system of a proline residue (Pro71) was also identified (Figure 2A,B). The unusual shift range can be interpreted in terms of a significant pseudocontact contribution to the shift of these resonances, consistent with the essentially axial position of this residue with respect to the heme moiety and the relatively short distances of its protons from the heme iron (within 6−9 Å). The assignment of Pro71 resonances is also supported by the observed interresidue NOESY connectivities. 1D NOE connectivities were also detected between the Hγ proton at 7.40 ppm and the two Hβs protons of Pro71 and the OH of Tyr67. Unusual shift values (which make their assignment nontrivial) were also observed for the resonances of the two heme-bound cysteines (Cys14, Cys17), the heme iron ligand His18 (Bren et al., 1995), Thr19, Asn31, Leu32, Ile35, Lys79, Ala80, and Ala81. All of them are located within a sphere of 9 Å from the heme iron.

Exchangeable side-chain protons were identified for Gln16, Asn31, Gln42, Tyr46, Tyr48 (the Hη of this residue was, however, observed only at 295 K), Thr49, Asn52, Asn56, Trp59, Asn62, Asn63, and Tyr67.

We already have reported the heme proton assignments (Bren et al., 1995). In the same paper we also discussed the long-range NOESY connectivities from heme methyls to other protein residues. Analogous interresidue NOESY connectivities (reported in Table 1) were also observed for propionate residues, for the thioether bridge resonances, and for the meso protons.

Information on the Secondary Structure. Once the backbone and side-chain proton assignments were obtained, the NOESY spectra were reexamined for the detection of medium-range-sequential NOEs (Figure 1). Backbone (i, i + 3) NOEs are indicative of α helical structure (Wüthrich, 1986). As reported in Figure 1, Hα−Hβ(i, i + 3) connectivities were observed for residues 4, 7, 8, 31, 50, 52, 63, 64, 71, 91, 95, 96, 98, and 100. Hα−NH(i, i + 3) connectivities were observed for residues 4, 5, 7, 8, 10, 15, 50−52, 61, 64, 65, 71, 89−91, and 94−98. Hα−NH(i, i + 4) connectivities, still indicative of a helix, were observed for residues 9, 11, 89, 95, 97, and 98. These data indicate the presence of α helical motifs for residues 4−15, 50−55, 61−68, 70−75, and 89−103. Backbone (i, i + 2) NOEs are indicators of 3_{10} helical elements (Wüthrich, 1986). Interestingly, NOESY connectivities of this kind are observed for several of the residues involved in the above discussed helices (see Figure 1), suggesting distortion of all the helices although at different extents. NH−NH(i, i + 2) NOEs were also observed for the 13−18 region, which contains the two thioether linkages to the heme (Cys14, Cys17) and the axial ligand of the iron (His18). Analysis of the data reported in Figure 1, therefore, establishes that the five helical elements present in all the characterized eukaryotic cytochromes *c* are retained in the Ala80cyt *c* variant. It is of interest to note that, as already reported for the noninhibited C102T yeast iso-1-cytochrome *c* (Gao et al., 1990), sequential NH−NH, Hα−NH, and Hβ−NH connectivities were observed also for the Phe-3Ser2 region. This can be taken as evidence that the N-terminal region possesses inherent structure in solution, although not of a helical type, as apparent from the lack of medium-range-sequential connectivities.

Table 1: Interresidue NOESY Connectivities Observed for Meso and Heme Pyrrole Substituent Resonances in the Cyanide Adduct of Ala80cyt *c*[a]

heme resonance	protein−residue resonance
2-Hα	Arg13 β's
	Cys14 β1
2-βCH_3	Arg13 β's
	Leu68 δ's
	Phe82 ζ, QR
	Leu85 δ's
	Leu94 δ's
4-Hα	Cys17 β2
	Val28 γ1
	Ala80 α
	Ala81 HN
4-βCH_3	Gln16 γ, ϵ's
	Val28 γ1
	Ala81 HN
6-Hα	Tyr46 ϵ2
6-Hα′	Tyr46 ϵ2
6-Hβ	Lys79 HN
	Ala80 HN, α, β
7-Hα	Asn52 δ1
	Trp59 ϵ1, ζ2
7-Hα′	Asn52 δ1
	Trp59 ϵ1, ζ2, η2
	Tyr67 ϵ1
7-Hβ	Leu32 δ's
	Tyr48 η
	Asn52 δ2
	Trp59 ϵ1, ζ2
7-Hβ′	Pro30 γ, δ
	Tyr48 ϵ1, η
α meso	Cys14 α
	Phe82 β
β meso	Ala80 α
	Ala81 HN
δ meso	Leu32 δ's
	Leu68 δ's
	Leu98 δ

[a] Taken from Bren et al. (1995).

Table 2: Number of Experimental and Meaningful Constraints Constituting the Upper Distance Limit File for Each Calibration Class

class	definition	no. of constraints (methyl peaks) exptl	meaningful
1	intraresidue (except HN, HA, HB)	504 (142)	274 (87)
2	sequential and intraresidue HN, HA, HB	601 (23)	418 (14)
3	medium range	106 (3)	106 (3)
4	long range backbone	22	22
5	long range	609 (269)	606 (269)
total no. of upper distance constraints		1842	1426

Solution Structure Determination

NOE Constraints. A total of 1834 experimental NOESY constraints were obtained using the program CALIBA. Eight additional distance constraints have been included from 1D NOE difference spectra obtained by saturating the hyperfine shifted signals of the ring protons of His18 and of the Tyr67 OH. The intensities of these connectivities were measured and properly scaled to those obtained from 2D experiments. Out of a total of 1842 experimental distance constraints, 1426 have been taken into account by DIANA and consequently by REM and RMD calculations. A total of 416 remaining constraints were found to be irrelevant for the calculation (i.e., either no conformation of the polypeptide chain could violate them or they correspond to fixed proton−proton distances). For protons without stereospecific assignments, pseudoatoms were used. The number of constraints transformed into upper distance limits are presented in Table 2 for each calibration class. The calibration was in agreement with the volume-to-distance correlation, when the intensities were assumed to be inversely proportional to the power of 4 of the corresponding upper distance limits in the case of classes 1, 3, 4, and 5 for protons and classes 1, 2, and 5 for methyls, to the power of 6 for class 2 for protons, and to the power of 5 for class 3 for methyls. Exponents lower than 6 are commonly found to give better calibration curves (Wüthrich, 1989; Güntert et al., 1991; Güntert & Wüthrich, 1991) as empirically take into account spin diffusion and possible contributions to the reorientational correlation time. The NOE constraints per residue are shown in Figure 3. With this number of distance constraints (which corresponds to 17.0 NOEs per residue as input for the DG calculation and 13.1 accepted experimental constraints per residue), a good-quality solution structure is expected (Clore & Gronenborn, 1994).

Definition of the Prosthetic Group for DG Calculations. The heme and the bound cyanide were included in the DG calculations through the addition of an artificial amino acid to the residue library used by the program DIANA (Güntert et al., 1991). A distance of 1.85 Å between the iron and the carbon of cyanide was set as that found in the X-ray structure of the cyanide adduct of cytochrome *c* peroxidase (Edwards & Poulos, 1990). The artificial residue, denoted by HES, consists of a histidine residue, whose Nϵ2 was connected to the heme skeleton through links with the four pyrrole nitrogens (upper distance limit 2.9 Å). As the DIANA library does not allow the introduction of metal ions, the heme iron was defined as a dummy atom, and its hexacoordinate geometry accomplished by imposing the appropriate upper and lower distance limits between this dummy atom and the ligand atoms by "special covalent bonds" (links). Starting from the four pyrrole nitrogens, the heme skeleton was built by defining normal covalent bonds between the atoms. The "special covalent bonds" were also used to define the link between the heme and Cys14 and Cys17: 2.1 and 1.9 Å were used as upper distance and lower distance limits, respectively, between the cysteine sulfur and the α-carbon of the corresponding heme thioether substituent. This yields a heme skeleton with the same distortion observed in the X-ray structure of yeast iso-1-cytochrome *c* (Louie et al., 1988; Louie & Brayer, 1990; Berghuis & Brayer, 1992). Defining the appropriate bonds as rotatable, the heme substituents have been allowed to assume all possible conformations. Analogously, the His18 ring can change its orientation with respect to the heme plane axes. Additional links between both carbon and nitrogen atoms of cyanide to the Nϵ2 of the His and the heme pyrrole nitrogens were introduced to maintain the cyanide ligand in the starting position.

Distance Geometry. The DG family obtained using distance constraints derived from dipole−dipole connectivities only consists of the 17 structures with the lowest target function (<0.3 Å^2) and with residual violation of the distance constraints, which does not exceed 0.2 Å. The distribution of the RMSD per residue inside the DG family (DG1, hereafter) for both backbone and heavy atoms is shown in Figure 4A and B, respectively (symbol ■). The average values of the RMSD within the DG1 family are 0.74 ± 0.10 and 1.35 ± 0.13 Å for backbone and heavy atoms, respectively (Table 3).

Two other distance geometry calculations were then performed. The input data of the first one (which generates the family indicated by DG2) differ from that described above only in the lack of the links between the heme and the sulfur atoms of Cys14 and Cys17. The removal of these heme−peptide linkages did not introduce any noticeable structural uncertainty within the set (see Table 3 and Figure 4, symbol ▲) or significant differences with respect to the DG1 family (the RMSD between the two average structures being ~0.2 Å for the backbone and ~0.3 Å for the heavy atoms). This is a clear indication that the experimental NOESY constraints are sufficient to produce the correct protein folding and that the presence of links between Cys14 and -17 and the heme during the DG calculations does not bias the protein structure. A minor difference is noted in the orientation of Cys17 side chain and 4-thioether β-CH_3.

A further DG calculation was performed including hydrogen bond constraints. This approach is widely used (Qi et al., 1994; Detlefsen et al., 1991; Markus et al., 1994), as further information involving exchangeable protons would help in better defining the solution structure. The final DG structure output of the calculation, which provided the DG1 family, was checked for possible hydrogen bonds involving both main-chain and side-chain atoms. The geometrical criteria we chose for the presence of a hydrogen bond requires the H-acceptor distance to be less than 2.4 Å and the angle formed by H, the donor atom, and the acceptor atom to be within 35°. For the main-chain atoms, these geometrical criteria were found to be satisfied in a set of 39 calculated structures (see Materials and Methods) for the following 21 NH/CO pairs: Gly6/Lys4, Phe10/Gly6, Lys11/Ala7, Thr12/Leu9, Leu15/Phe10, Cys17/Cys14, His18/Cys14, Lys54/Asp50, Tyr67/Asn63, Leu68/Met64, Tyr74/Asn70, Ile75/Pro71, Leu94/Asp90, Ile95/Arg91, Thr96/Asn92, Tyr97/Asp93, Leu98/Leu94, Lys99/Ile95, Lys100/Thr96, Ala101/Tyr97, and Ser102/Leu98. Consistent hydrogen

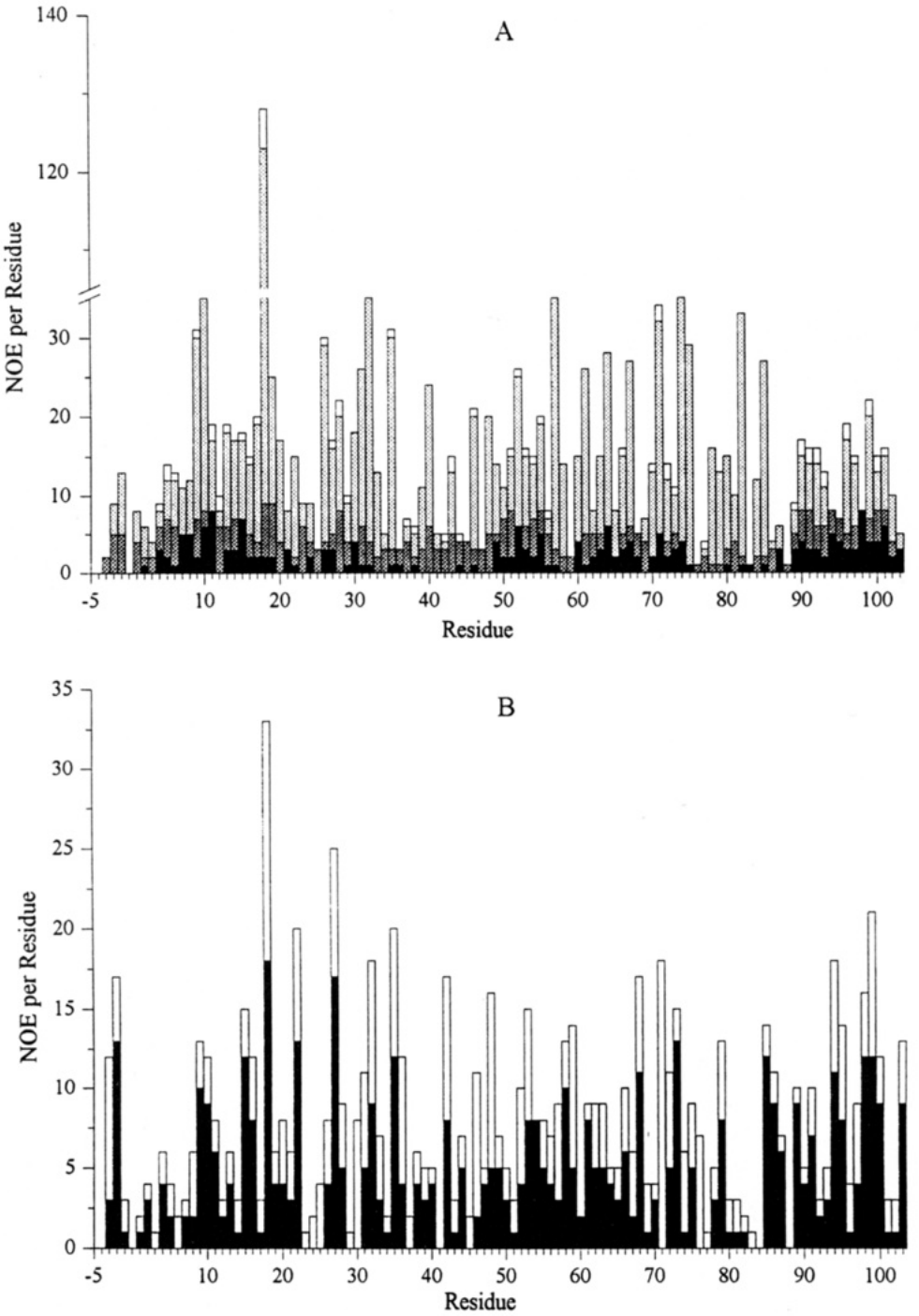

FIGURE 3: Number of inter- (A) and intraresidual (B) NOEs per residue identified in the NMR spectra of the cyanide adduct of Ala80cyt *c*. The total height of each column represents the amount of the observed experimental NOEs. In panel A, the black bars correspond to class 2 NOE constraints, dark-shaded bars correspond to class 3 NOE constraints, light shaded bars correspond to class 4 and 5 NOE constraints, and the open bars correspond to irrelevant constraints. In panel B, open and filled bars correspond to intraresidue NOE constraints which are found to be irrelevant and meaningful, respectively.

bonds are also present for the pairs His18 Hδ1/Pro30 CO, Val57 NH/Ser40 Oγ, NH Gly1/Oγ1 Thr96, and NH Ala43/Oη Tyr48. Among these, the presence of hydrogen bonds involving the amide protons of residues 1, 10, 11, 12, 15, 43, 68, 75, 94, 95, 97, 98, 99, 101, and 102 is supported by the experimental observation that the corresponding resonances are still present in the spectra recorded 4 weeks after the lyophilized sample was dissolved in D_2O solution. Slow exchange was experimentally observed also for the NH proton of the Trp59 indole ring. This proton falls within hydrogen bond distance from the O2 atom of heme-propionate 7. The same O2 atom falls within H-bond distance from two other exchangeable protons, i.e., NH of Gly 41 and Hδ2 of Asn52, but experimental evidence for slow exchange was found for the amide proton of Gly41 only. All these hydrogen bonds involving slowly exchanging protons were incorporated as constraints setting the distances between the H and the acceptor atom less than 2.4 Å and the distance between the donor and the acceptor atoms in the range 2.7−3.4 Å (i.e., to maintain the angle H−donor−acceptor within 62°). For the Hϵ1 of Trp59 and the O2 atom of propionate-7 only the donor−acceptor distance was allowed to range between 2.7 and 3.7 Å. The average RMSD values for the resulting family (DG3) are reported in Table 3, whereas the RMSD per residue are reported in Figure 4 (symbol $\triangledown$). As a general improvement in the RMSD values

Table 3: Average RMSD Values for Backbone (BB) and for All Heavy Atoms (HA) for the DG1,[a] DG2,[a] DG3,[a] and REM Families of Structures of the Cyanide Adduct of Ala80cyt *c*[a]

	DG1	DG2	DG3	REM
RMSD for residues Gly1−Ser102 (Å)				
BB	0.74 ± 0.10	0.72 ± 0.10	0.70 ± 0.11	0.68 ± 0.11
HA	1.35 ± 0.13	1.34 ± 0.12	1.32 ± 0.13	1.32 ± 0.14
target function (Å^2)	0.24	0.39	0.33	
total distance violations (Å)			3.9	4.2
total energy (kJ mol^{-1})				−6712.6
deviation from ideal bond distances (Å)				0.008
deviation from ideal bond angles (deg)				1.60

[a] DG1, DG2, and DG3 represent the 17 individual structures obtained from DG calculations, from DG calculations excluding the constraints of the links between heme and Cys14 and Cys17, and from DG calculations including hydrogen bond constraints, respectively. [b] For the last family, the average energy values are also reported.

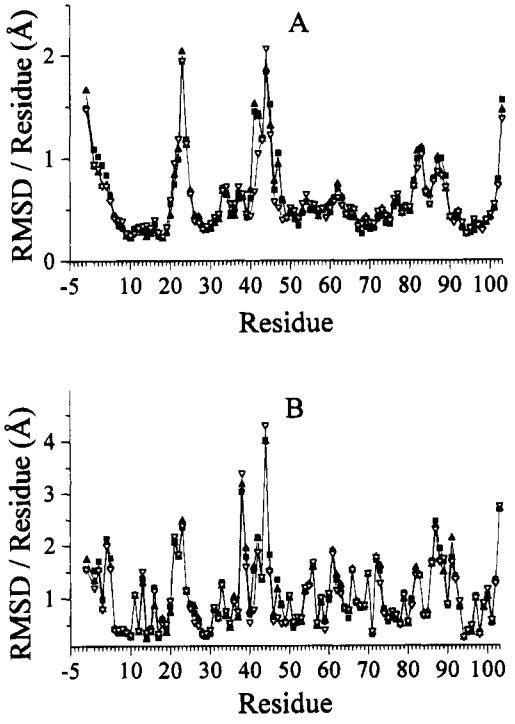

FIGURE 4: Diagrams of the RMSD values per residue for the 17 accepted structures of the cyanide adduct of Ala80cyt *c* for DG1 (■), DG2 (▲), and DG3 (▽). RMSD values for the backbone and heavy atoms are presented in panels A and B, respectively.

is observed upon introduction of the H-bond constraints, the DG3 family was then used for structural refinements.

Restrained Energy Minimization and Restrained Molecular Dynamics. The 17 structures of the DG3 family were used as starting structures for the REM calculations. The mean global RMSD values for residues 1−102 in the REM family for the backbone and all heavy atoms are 0.68 ± 0.11 and 1.32 ± 0.14 Å, respectively (Table 3). In Figure 5A,B (symbol ◇), the distribution of the RMSD per residue (backbone and heavy atoms) is compared to that obtained for the DG3 family. The stereodrawings of the DG3 and REM families (backbone, heme moiety, His18 ligand) are shown in Figure 6A and B, respectively.

RMD calculations were then performed on the REM family. The last 24 ps of the MD trajectory for each structure was used to generate an average structure which was then energy minimized to obtain the RMD family. The average RMSD values for the RMD family are 0.76 ± 0.12 and 1.45 ± 0.17 Å for the backbone and all heavy atoms, respectively, i.e., somewhat worse than those of the REM family. It is possible that the force constant is not sufficient to provide a narrow family for the present number of constraints. This

Table 4: Statistical Analysis Derived from the 17 Calculated Structures Obtained by the DG Calculation (DG3) and Restrained Energy Minimization (REM)[a]

	RMSDs (Å)	
comparison	backbone	heavy atoms
DG3 vs ⟨DG3⟩	0.47 ± 0.08	0.91 ± 0.09
REM vs ⟨REM⟩	0.51 ± 0.07	0.94 ± 0.08
⟨DG3⟩ vs ⟨REM⟩	0.38	0.55

[a] DG3 and REM refer to the 17 individual structure families. ⟨DG3⟩ and ⟨REM⟩ are the mean structures obtained by averaging the coordinates of the DG3 and REM structures, respectively. The RMSD values were calculated with respect to the mean structure. For all the comparisons, residues from 1 to 102 are considered.

may also contain some information on the mobility and/or flexibility of the protein. These aspects may be further analyzed in the future.

Evaluation of the Structure Quality. The RMSD values reported in Table 3 indicate that there is only a small improvement in the structure definition going from DG3 to REM. From inspection of Figure 6 it is evident that the conformations of two families are essentially the same.

The presence of α helices has been checked with the program Procheck (Laskowski et al., 1993). In the two families DG3 and REM, the residues 6−11, 50−55, 61−70, 71−75, and 89−101 have been found to form α helices.

The N-terminal residues show relatively large RMSD values in all the families. A substantial disorder for these residues has also been observed in the X-ray crystal structure of yeast iso-1-cytochrome *c* in both oxidation states (Berghuis & Brayer, 1992) and may, at least partially, account for the lack of increased structure resolution from DG3 to REM and for an increased disorder when passing to RMD. The residues involved in the first α helix are characterized by low RMSD values in the DG3 and the REM families (0.40 and 0.37 Å, respectively).

Very low RMSD values for the two families (0.32 and 0.27 Å in DG3 and REM) are found for residues 14−19, which include the heme-bound residues Cys14 and Cys17 and the iron-bound His18.

The residues 21−24 are characterized, in the DG3 and in the REM families, by larger RMSD values (the largest values being 1.95 and 1.94 Å for residue 23, in DG3 and REM, respectively). Indeed, the number of interresidue NOEs for the residues in this part of the protein is low, being on average 10.2. RMD calculations drastically reduce the RMSD values (1.0 Å for residue 23).[1]

The 25−36 protein region is characterized by RMSD values lower than that for the whole protein (0.49 and 0.40 Å in DG3 and REM). The following 37−47 region is, to

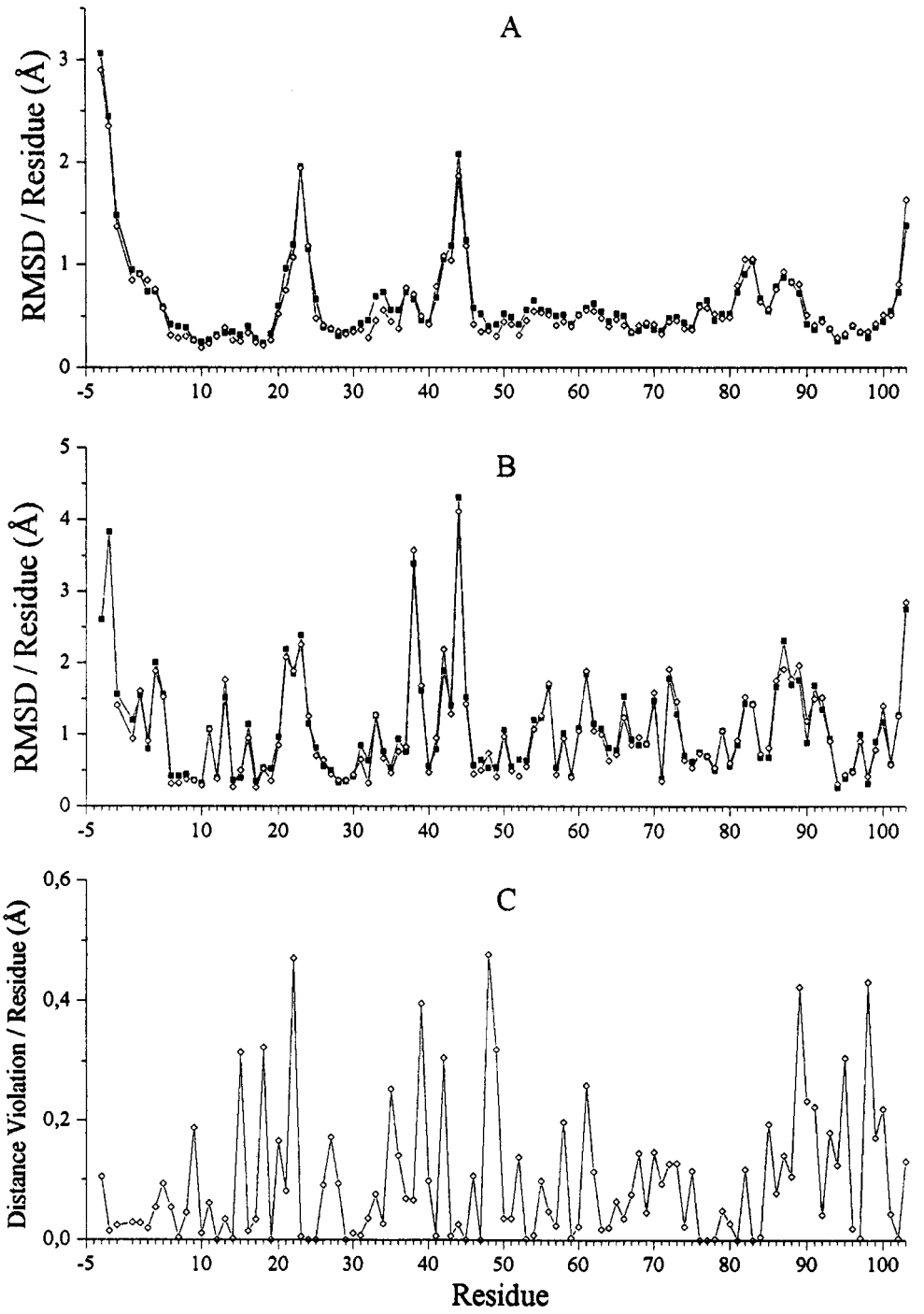

FIGURE 5: Diagrams of the RMSD per residue for the 17 accepted structures of the cyanide adduct of Ala80cyt *c* that constitute the DG3 (■) and REM (◇) families. RMSD values for the backbone and the heavy atoms are presented in panels A and B, respectively. Panel C shows the average value of the distance violation per residue reported by SANDER after REM.

the contrary, characterized by the highest RMSD values of all the protein. This protein region is indeed characterized by a low number of interresidue NOEs (9.6 on average). This is due to the structural properties of this segment of the protein: it does not have any secondary structure element and is projected toward the outside of the protein, forming an external loop. Therefore, fewer interresidue NOEs are expected.

The 48−80 region is well defined in all three families, with RMSD values lower than the average values (0.49 Å in DG3 and 0.48 Å in REM). As discussed above, three helices can be identified (residues 50−55, 61−70, and 71−75) in this part of the protein. Between residues 81 and 88, a slight increase in the spreading of the families (RMSD values for DG3 and REM being 0.80 and 0.83 Å) is observed. The relatively low number of interresidue NOEs in this part of the protein can be ascribed mainly to the lower number of assignments with respect to the other residues in the protein.

At the C-terminus a long α helix is present, which is very well defined in all families. The calculated RMSD values

[1] The spreading of the structures in this protein region for the RMD family is drastically reduced with respect to the other families. The structures, therefore, even if not very well defined in terms of NOEs, are able when relaxed during MD calculations to find conformations at minimum energy that are close each other.

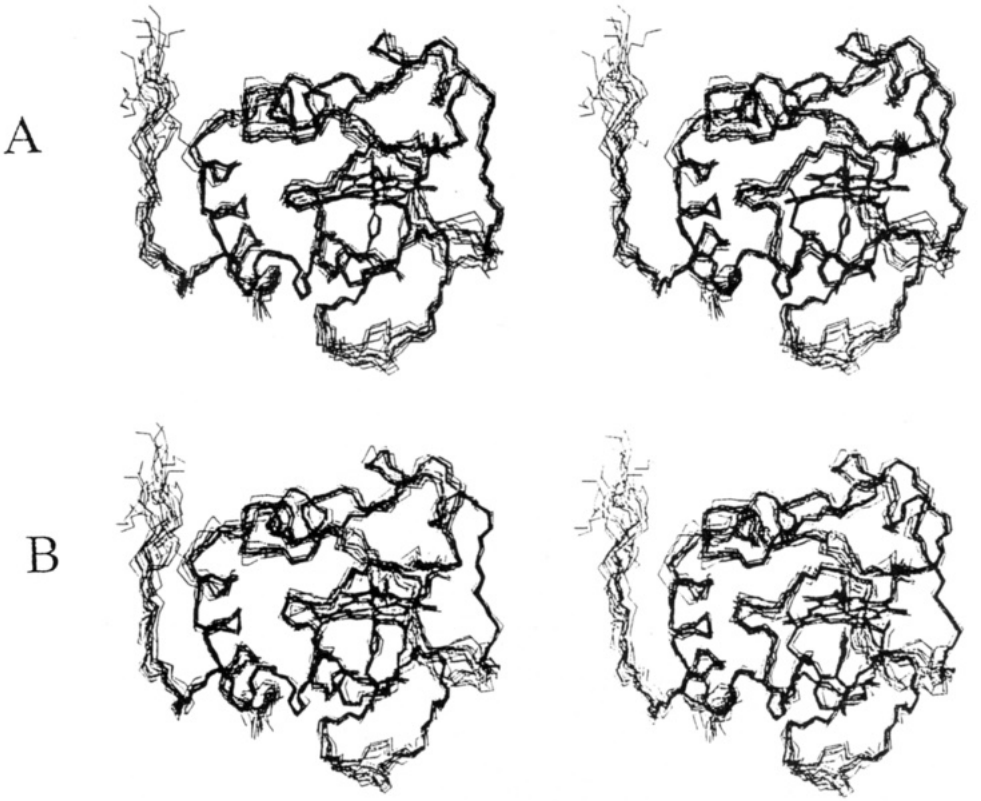

FIGURE 6: Stereo drawings of the 17 accepted structures of the cyanide adduct of Ala80cyt *c* that constitute the DG3 (A) and REM (B) families.

for the 89−102 residues are 0.43 and 0.47 Å in DG3 and REM, respectively.

The trend of the RMSD values found for the backbone atoms is observed also for the heavy atoms. The highest RMSD values are still found for residues 21, 22, 23, 38, 42, and 44. The 50−80 region, which is characterized by the lowest average RMSD values, shows, however, larger fluctuations in these values with respect to the behavior of the backbone atoms.

It is interesting to compare the pattern of the RMSD values per residue with the penalty of the distance constraints, found after the REM calculations (Figure 5C). Large penalty values do not correspond to violations in the DG calculations and are introduced by the coordinate variations which are allowed for the protein atoms during the energy minimization calculations. The total distance violation in the REM family is very low (4.2 Å), which corresponds to an average value per residue of 0.04 Å. The individual distance violations are always lower than 0.28 Å. The largest penalty values are found for residues 22, 48, 89, and 98 (Figure 5C). The total penalty energy for these violations is 72.9 kJ mol^{-1}.

Another relevant parameter for the definition of the quality of the structure, which can provide further insight in the analysis of the three families, is given by the order parameter *S*. This parameter is 0 for randomly oriented structures while it is 1 for perfectly superimposed structures. The $1 - S$ quantity is therefore a measure of the disorder of the structures within a family. In Figure 7, we report the quantity $1 - S$ per residue evaluated for the ϕ, ψ, and $\chi 1$ angles, i.e., for the the CO_{i-1}-N_i-C_i-CO_i (backbone), N_i-C_i-CO_i-N_{i+1} (backbone) and N_i-C_i-C_i-X_i (backbone−beginning of the side chain) dihedral angles, respectively. For the ψ angle, a general improvement is observed going from DG3 to REM. This is particularly sizable for the 20−27 range. The $1 - S$ parameter for the ϕ and $\chi 1$ angles does not show meaningful changes between the two families, although there is a slight decrease in its absolute value.

The analysis of the Ramachandran plot, which reports the values of the ψ and φ dihedral angles, is another tool we used to check the quality of the structures. In the REM average structure, 69 residues over a total of 90 "meaningful" residues, i.e., non-glycine, non-proline, and nonterminal residues (i.e., 76.7% of the meaningful residues) fall in the most favored regions, with 18 residues (i.e., 20.0%) in additional allowed regions. Asn56 (i.e., 1.1%) falls in the generously allowed regions, while Lys5 and Glu88 (2.2%) are in the disallowed regions. Given the resolution of the present structure (~2.5 Å according to a rough equivalence criterion between NMR and X-ray structures (Clore & Gronenborn, 1994)), the percentage of residues in the most favored regions is in the range expected for a good quality structure.

Most of the side chains appear to have the same orientation in the two families. Phe-3 is characterized by large RMSD values in the two families. The high disorder of Phe-3 seems to be in contrast with the large number (33) of interresidue NOEs observed for the ring protons of this residue. However, with the calibration we used, most of them correspond to a very long upper distance limit, thus giving poor overall constraints for this residue. This suggests that the N-terminal part of the protein is probably characterized by a different mobility with respect to the rest of the protein, which would require the use of a special calibration. As discussed above, this part of the protein chain also appears to be characterized by large mobility (large thermal factors) in the X-ray structure.

Most of the charged side chains (Lys, Arg, Glu, Asp) point toward the exterior. They maintain the same orientation in DG3 and REM. An electrostatic interaction between Asp50 and Lys54 is observed in REM.

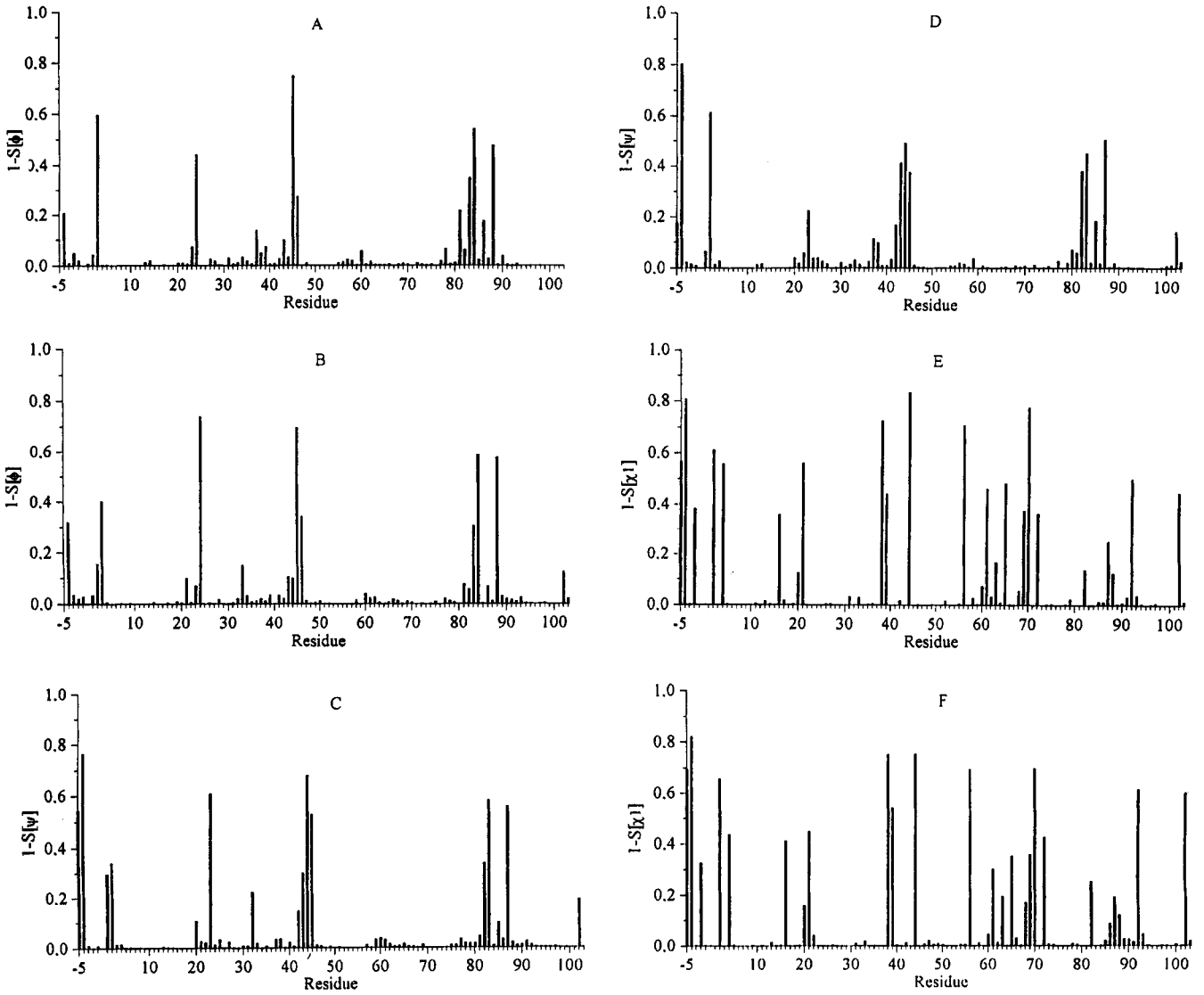

FIGURE 7: Diagrams of the $1 - S$ parameter for the 17 structures of the cyanide adduct of Ala80cyt c for the DG3 and REM families. Histograms of the $1 - S$ parameter values of the ϕ, ψ, and $\chi 1$ angles in the DG3 and REM families are presented in panels A, C, E, and B, D, F, respectively.

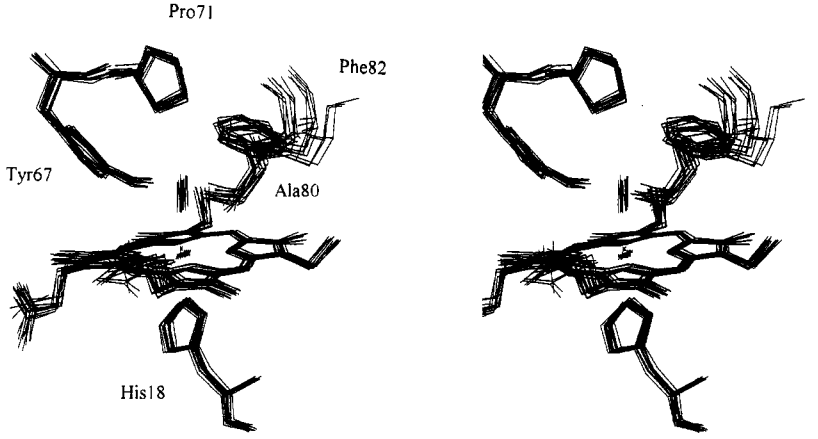

FIGURE 8: Stereo drawing of the active site cavity as it results in the 17 structures of the REM family. The H-atom of the OH group of Tyr67 is also displayed to show the H bond with the nitrogen atom of cyanide. The covalent bonds between the heme iron and the axial ligands are not displayed.

Particular attention should be devoted to the analysis of the definition of the structure of the heme, the heme-bound cysteines, the iron-bound histidine, and the residues in the "distal cavity" where the mutated Ala80 residue is present. From inspection of the RMSD values (Figure 5A,B), of the $1 - S$ parameters (Figure 7), and of the distance violations (Figure 5C) for these residues, it is clear that this part of the protein is better defined than the average. A special comment can be made in reference to the OH of Tyr67. The presence of a hydrogen bond between this proton and the

Table 5: RMSD Values for Backbone (BB) and for Heavy Atoms (HA) of the X-ray Crystal Structure of the Wild-Type Yeast Iso-1-cytochrome *c* in Both Oxidation States with Respect to the Average Solution Structure of the Cyanide Adduct of Ala80cyt *c* Calculated for DG3 and REM Families[a]

	RMSD for residues Gly1−Ser102 (Å)	
	<DG3>	<REM>
ferroform		
BB	1.10	0.95
HA	1.64	1.50
ferriform		
BB	1.13	0.99
HA	1.71	1.60

[a] The RMSD values are calculated for the 1−102 residue range.

nitrogen of the cyanide ligand was proposed (Bren et al., 1995) on the basis of its short T_1 value (~9 ms), which places it ~4 Å from the heme iron, and its slow exchange with bulk water. The analogy with the role of the distal His Hε2 in the cyanide adducts of metmyoglobin and peroxidases has already been stressed. Indeed, in all the calculated structures, this proton falls within hydrogen bond distance from the nitrogen atom of cyanide, although the angle requirement is not always fulfilled. The structural arrangement of the Tyr67 ring is shown in Figure 8 for the REM. The OH proton, which is located at 2.2 Å from the N atom of the cyanide ligand, has the same orientation for all members of the family. No differences are observed between REM and RMD families for this residue.

Comparison with the Solution Structure of Horse Heart Cytochrome c. In Table 4, the average RMSD values between each component of the DG3 family with the mean DG3 structure, ⟨DG3⟩, are reported. The values of 0.47 ± 0.08 Å for the backbone and 0.91 ± 0.09 Å for the heavy atoms indicate that the structure quality is at the same level as that of the recently reported solution structure of horse heart ferrocytochrome *c* (RMSD values about the average structure of 0.47 ± 0.09 and 0.91 ± 0.07 Å for the backbone and the heavy atoms, respectively) (Qi et al., 1994). The presence of the paramagnetic center, therefore, does not affect the structure resolution. Residues 23 and 24 also are reported to have the largest RMSD values in the solution structure of the horse heart protein.

Comparison of the X-ray and Solution Structures. A comparison of the X-ray structure of yeast iso-1-cytochrome *c* in both oxidation states (the structure of the oxidized form being on the Cys102Ser mutant) (Berghuis & Brayer, 1992; Louie et al., 1988; Louie & Brayer, 1990) with ⟨DG3⟩ and ⟨REM⟩ families is reported in Table 5 in terms of RMSD values. The distribution of the RMSD for backbone and heavy atoms for the average ⟨DG3⟩ (symbol ■) and ⟨REM⟩ (symbol ◇) structures with respect to the X-ray structure of the ferri form is reported in Figure 9. The residues that most deviate from the X-ray structure correspond to those with the largest RMSD values within the families (Figures 5 and 6). The side chains of the aromatic residues have, overall, similar orientations in the X-ray structure of wild-type cyt *c* and in the solution structures of the Ala80cyt *c* variant. The ring of Phe10 (which is very well defined in the solution structure with an RMSD value for the heavy atoms of 0.29 Å) has the same orientation but experiences a small translation. Phe82 is located above the heme ring in the "distal" pocket, on the solvent-exposed heme side. It forms a hole toward the solvent which is ~4 Å wide in the X-ray structure.

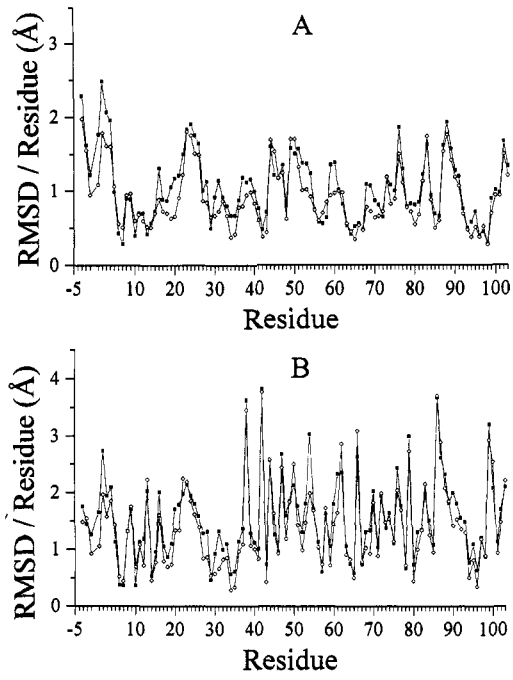

FIGURE 9: Diagrams of the RMSD values per residue for the average <DG3> (■) and <REM> (◇) structures with respect to the X-ray structure of Cys102Ser yeast iso-1-ferricytochrome *c*. RMSD values for the backbone and heavy atoms are presented in panels A and B, respectively. In the case of residue 39, the comparison with the X-ray structure for the heavy atoms is not meaningful because in the present variant we have Gln39 instead of His39.

In the solution structure, the ring of Phe82 has an average position closer to the heme but the movement is within the resolution of the residue. Also, the side chains of charged residues, which have been proposed to be involved in interactions with physiological partners (Moore & Pettigrew, 1990; Pettigrew & Moore, 1987), have very similar orientations in the two structures. Significantly, very small RMSD values are observed for residue 18 (i.e., the HES amino acid constituted by the His18 and the heme), as well as for the two heme-bound cysteines (Cys14, Cys17). Indeed, the proximal His orientation observed in the solution structure is essentially unchanged from the X-ray structure of wild-type cyt *c*. Among the residues present in the "distal site," the backbone and heavy atoms of Pro71 experience very small RMSD values. Therefore, although the shift values for the proton resonances of this residue are very different from those previously reported for the noninhibited wild-type yeast iso-1-cytochrome *c* (Gao et al., 1990), they cannot be related to meaningful structural differences, but seem to be due to different pseudocontact contributions to the hyperfine shifts arising from a different orientation of the magnetic axes. For Tyr67, the RMSD value between the X-ray and the ⟨REM⟩ structure also is very small (0.47 and 0.79 Å, for the backbone and all heavy atoms, respectively). This means that the location and orientation of this residue is the same as in the X-ray structure of wild-type cytochrome *c*. However, based on the ^{1}H NMR data reported on the wild-type protein (Qi et al., 1994; Wand et al., 1989; Moore & Williams, 1980a,b), the dynamics of this residue appear to be different. Tyr67 in the wild-type protein forms a hydrogen bond with the sulfur atom of Met80, whereas in the cyanide derivative it forms a hydrogen bond with the cyanide moiety. The flipping rate of the ring is reduced in the mutant. The backbone of the segment 79−81, which

includes the modified Ala80 residue, is essentially the same in the two structures.

The substitution of the long side chain of Met80 with the short one of an alanine produces a large cavity on the "distal" side of the heme. In this mutant, no heavy atoms belonging to protein residues are present within ~6.5 Å of the iron. In myoglobin, the distal cavity is smaller, the iron having no heavy atoms of protein residues within ~5 Å (Kuriyan et al., 1986), while this radius in peroxidases is in the 5.5–6 Å range (Edwards et al., 1993; Smith et al., 1983; Poulos & Kraut, 1980; Finzel et al., 1984; Edwards & Poulos, 1990).

On the basis of the comparison of the dioxygen-binding properties of myoglobin mutants and those of Ala80cyt *c*, it was proposed that Phe82 may play a role in dioxygen stabilization (Bren & Gray, 1993). In a model structure of the Ala80 variant, Phe82 was rotated from its position in the native structure to show the potential Phe–O_2 interaction (Bren & Gray, 1993). The present solution structure shows that the Phe ring is not pointing toward the cyanide moiety. However, the 3.3 Å distance from the Phe82 δ-carbon to the cyanide nitrogen compares with the 3.2 Å distance seen between the O(2) atom of dioxygen and the ζ-carbon of Phe29 (position B10) in the X-ray structure of Leu29Phe sperm whale myoglobin (Carver et al., 1992). The remarkable stability of dioxygen adduct of Leu29Phe myoglobin has been attributed to this interaction. Our results show that this type of interaction may occur in Ala80cyt *c*. The major distal cavity interaction involved in stabilization of of Ala80cyt $c-O_2$ is likely hydrogen bonding from the Tyr67 OH to the iron-bound dioxygen. Interestingly, a similar interaction between O_2 and the position B10 tyrosine is believed to be responsible for the exceptionally strong binding of O_2 to *Ascaris* hemoglobin (De Baere et al., 1994; Kloek et al., 1994). The resistance of the dioxygen adduct of Ala80cyt *c* to oxidation is likely related to the iron site being protected by the protein matrix (Bren & Gray, 1993). The similarity of the overall structure of Ala80cyt *c* to that of native cyt *c* confirms that this is a property of the cytochrome *c* fold.

ACKNOWLEDGMENT

We thank Yi Lu for helpful discussions. K.L.B. acknowledges a Kodak graduate fellowship. P.S. acknowledges the Italian Ministry of Foreign Affairs for a Ph.D. grant. This work was supported by the EC Biotechnology Program BIO2-CT94-2052 (DG12SSMA), the CNR (Italy), and the National Science Foundation (United States). This work has been performed with the instrumentation of the Florence Laboratory of Relaxometry and Magnetic Resonance on Paramagnetic Metalloproteins, Large Scale Facility of the European Community.

SUPPORTING INFORMATION AVAILABLE

A table containing the proton assignment for the cyanide adduct of Ala80cyt *c* (shift values measured at 303 K) and a listing of the experimental NOE and NOESY intensities as well as of the hydrogen bond constraints used for the structure calculation (22 pages). Ordering information is given on any current masthead page.

REFERENCES

Angelucci, L., De Gioia, L., & Fantucci, P. (1993) *Gazz. Chim. Ital. 123*, 111–117.
Argos, P., & Mathews, F. S. (1975) *J. Biol. Chem. 250*, 747–751.
Banci, L., Bertini, I., Luchinat, C., Piccioli, M., Scozzafava, A., & Turano, P. (1989) *Inorg. Chem. 28*, 4650–4656.
Banci, L., Bertini, I., & Luchinat, C. (1991a) *Nuclear and Electron Relaxation. The Magnetic Nucleus-Unpaired Electron Coupling in Solution*, VCH, Weinheim.
Banci, L., Bertini, I., Turano, P., Ferrer, J. C., & Mauk, A. G. (1991b) *Inorg. Chem. 30*, 4510–4516.
Banci, L., Bertini, I., Turano, P., Tien, M., & Kirk, T. K. (1991c) *Proc. Natl. Acad. Sci. U.S.A. 88*, 6956–6960.
Banci, L., Bertini, I., Pease, E. A., Tien, M., & Turano, P. (1992) *Biochemistry 31*, 10009–10017.
Banci, L., Bertini, I., Eltis, L. D., & Pierattelli, R. (1993a) *Biophys. J. 65*, 806–813.
Banci, L., Bertini, I., Kuan, I.-C., Tien, M., Turano, P., & Vila, A. J. (1993b) *Biochemistry 32*, 13483–13489.
Banci, L., Carloni, P., & Gori Savelini, G. (1994) *Biochemistry 33*, 12356–12366.
Bax, A., & Freeman, R. (1981) *J. Magn. Reson. 44*, 542–561.
Bax, A., & Davis, D. G. (1985) *J. Magn. Reson. 65*, 355–360.
Bax, A., Freeman, R., & Morris, G. (1981) *J. Magn. Reson. 42*, 164–168.
Berendsen, H. J. C., Postma, J. P. M., van Gunsteren, W. F., DiNola, A., & Haak, J. R. (1984) *J. Chem. Phys. 81*, 3684–3690.
Berghuis, A. M., & Brayer, G. D. (1992) *J. Mol. Biol. 223*, 959–976.
Bertini, I., & Luchinat, C. (1986) *NMR of Paramagnetic Molecules in Biological Systems*, Benjamin/Cummings, Menlo Park, CA.
Bertini, I., Turano, P., & Vila, A. J. (1993) *Chem. Rev. 93*, 2833–2932.
Bertini, I., Dikiy, A., Luchinat, C., Piccioli, M., & Tarchi, D. (1994) *J. Magn. Reson. Ser. B 103*, 278–283.
Blackledge, M. J., Medvedeva, S., Pomein, M., Guerlesquim, F., Bruschi, M., & Marion, D. (1995) *J. Mol. Biol. 245*, 661–681.
Bren, K. L., & Gray, H. B. (1993) *J. Am. Chem. Soc. 115*, 10382–10383.
Bren, K. L., Gray, H. B., Banci, L., Bertini, I., & Turano, P. (1995) *J. Am. Chem. Soc.*, in press.
Carver, T. E., Brantley, R. E., Jr., Singleton, E. W., Arduini, R. M., Quillin, M. L., Phillips, G. N., Jr., & Olson, J. S. (1992) *J. Biol. Chem. 267*, 14443–14450.
Case, D. A., & Karplus, M. (1979) *J. Mol. Biol. 132*, 343–368.
Clore, G. M., & Gronenborn, A. M. (1994) *Protein Sci. 3*, 372–390.
Dawson, J. H., Andersson, L. A., & Sono, M. (1982) *J. Biol. Chem. 257*, 3606.
De Baere, I., Perutz, M. F., Kiger, L., Marden, M. C., & Poyart, C. (1994) *Proc. Natl. Acad. Sci. U.S.A. 91*, 1594–1597.
de Ropp, J. S, La Mar, G. N., Wariishi, H., & Gold, M. H. (1991) *J. Biol. Chem. 266*, 15001–15008.
Detlefsen, D. J., Thanabal, V., Pecoraro, V. L., & Wagner, G. (1991) *Biochemistry 30*, 9040–9046.
Eccles, C., Güntert, P., Billeter, M., & Wüthrich, K. (1991) *J. Biomol. NMR 1*, 111–130.
Edwards, S. L., & Poulos, T. L. (1990) *J. Biol. Chem. 265*, 2588.
Edwards, S. L., Raag, R., Wariishi, H., Gold, M. H., & Poulos, T. L. (1993) *Proc. Natl. Acad. Sci. U.S.A. 90*, 750–754.
Egeberg, K. D., Springer, B. A., Sligar, S. G., Carver, T. E., Rohlfs, R. J., & Olson, J. S. (1990) *J. Biol. Chem. 265*, 11788–11795.
Emerson, S. D., & La Mar, G. N. (1990) *Biochemistry 29*, 1545–1556.
Ferrer, J. C., Turano, P., Banci, L., Bertini, I., Morris, I. K., Smith, K. M., Smith, M., & Mauk, A. G. (1994) *Biochemistry 33*, 7819–7829.
Finzel, B. C., Poulos, T. L., & Kraut, J. (1984) *J. Biol. Chem. 259*, 13027–13036.
Gao, Y., Boyd, J., Williams, R. J. P., & Pielak, G. J. (1990) *Biochemistry 29*, 6994–7003.
Griesinger, C., Otting, G., Wüthrich, K., & Ernst, R. R. (1988) *J. Am. Chem. Soc. 110*, 7870–7872.
Güntert, P., & Wüthrich, K. (1991) *J. Biomol. NMR 1*, 447–456.
Güntert, P., Braun, W., & Wüthrich, K. (1991) *J. Mol. Biol. 217*, 517–530.
Güntert, P., Berndt, K. D., & Wüthrich, K. (1993) *J. Biomol. NMR 3*, 601–606.
Hancock, R. D. (1989) in *Progress in Inorganic Chemistry* (Lippard, S. J., Ed.) Vol. 37, p 187, John Wiley & Sons, Inc., New York.

Inubushi, T., & Becker, E. D. (1983) *J. Magn. Reson. 51*, 128−133.
Jones, L. H. (1971) *Inorganic Vibrational Spectroscopy*, Marcel Dekker, New York.
Kloek, A. P., Yang, J., Mathews, F. S., Frieden, C., & Goldberg, D. E. (1994) *J. Biol. Chem. 269*, 2377−2379.
Kuriyan, J., Wilz, S., Karplus, M., & Petsko, G. A. (1986) *J. Mol. Biol. 192*, 133−154.
La Mar, G. N., Chen, Z. G., Vyas, K., & McPherson, A. D. (1995) *J. Am. Chem. Soc. 117*, 411−419.
Laskowski, R. A., MacArthur, M. W., Moss, D. S., & Thornton, J. M. (1993) *J. Appl. Crystallogr. 26*, 283−291.
Louie, G. V., & Brayer, G. D. (1990) *J. Mol. Biol. 214*, 527−555.
Louie, G. V., Hutcheon, W. L. B., & Brayer, G. D. (1988) *J. Mol. Biol. 199*, 295−314.
Lu, Y., Casimiro, D. R., Bren, K. L., Richards, J. H., & Gray, H. B. (1993) *Proc. Natl. Acad. Sci. U.S.A. 90*, 11456−11459.
Macura, S., Wüthrich, K., & Ernst, R. R. (1982) *J. Magn. Reson. 47*, 351−357.
Marion, D., & Wüthrich, K. (1983) *Biochem. Biophys. Res. Commun. 113*, 967−974.
Markus, M. A., Nakayama, T., Matsudaira, P., & Wagner, G. (1994) *Protein Sci. 3*, 70−81.
Moore, G. R., & Williams, R. J. P. (1980a) *Eur. J. Biochem. 103*, 513−522.
Moore, G. R., & Williams, R. J. P. (1980b) *Eur. J. Biochem. 103*, 523−532.
Moore, G. R., & Pettigrew, G. W. (1990) *Cytochromes c; Evolutionary, Structural and Physicochemical Aspects*, Springer-Verlag, Berlin.
Nakamoto, K. (1978) *Infrared and Raman Spectra of Inorganic and Coordination Compounds*, John Wiley & Sons, New York.
Nakamoto, K., Takemoto, J., & Chow, T. L. (1971) *Appl. Spectrosc. 25*, 352−355.
Pearlman, D. A., Case, D. A., Caldwell, G. C., Siebel, G. L., Singh, U. C., Weiner, P., & Kollman, P. A. (1991) *AMBER 4.0*, University of California, San Francisco.
Pettigrew, G. W., & Moore, G. R. (1987) *Cytochromes c; Biological Aspects*, Springer-Verlag, Berlin.
Poulos, T. L., & Kraut, J. (1980) *J. Biol. Chem. 255*, 8199−8205.
Qi, P. X., Di Stefano, D. L., & Wand, A. J. (1994) *Biochemistry 33*, 6408−6417.
Rohlfs, R. J., Mathews, A. J., Carver, T. E., Olson, J. S., Springer, B. A., Egeberg, K. D., & Sligar, S. G. (1990) *J. Biol. Chem. 265*, 3168−3176.
Ross, W. S. (1994) *CARNAL*, Department of Pharmaceutical Chemistry, University of California, San Francisco.
Ruf, H. H., Wende, P., & Ullrich, V. (1979) *J. Inorg. Biochem. 11*, 189−204.
Satterlee, J. D., & Erman, J. E. (1980) *Arch. Biochem. Biophys. 202*, 608−616.
Satterlee, J. D., & Erman, J. E. (1991) *Biochemistry 30*, 4398−4405.
Satterlee, J. D., Erman, J. E., Mauro, J. M., & Kraut, J. (1990) *Biochemistry 29*, 8797−8804.
Satterlee, J. D., Russell, D. J., & Erman, J. E. (1991) *Biochemistry 30*, 9072−9077.
Sayle, R. (1994) Biomolecular Structure Department, Glaxo Research and Development, Greenford, Middlesex, U.K.
Sette, M., de Ropp, J. S., Hernandez, G., & La Mar, G. N. (1993) *J. Am. Chem. Soc. 115*, 5237−5245.
Smerdon, S. J., Dodson, G. G., Wilkinson, A. J., Gibson, Q. H., Blackmore, R. S., Carver, T. E., & Olson, J. S. (1991a) *Biochemistry 30*, 6252−6260.
Smerdon, S. J., Krzywda, S., Wilkinson, A. J., Gibson, Q. H., Blackmore, R. S., Dezz Ropp, J., & Sligar, S. G. (1991b) *Biochemistry 30*, 4697−4705.
Smith, T. D., Gaunt, R., & Ruzic, I. (1983) *Inorg. Chim. Acta 78*, 103−106.
Springer, B. A., Egeberg, K. D., Sligar, S. G., Rohlfs, R. J., Mathews, A. J., & Olson, J. S. (1989) *J. Biol. Chem. 264*, 3057−3060.
Thanabal, V., & La Mar, G. N. (1989) *Biochemistry 28*, 7038−7044.
Unger, S. W., Lecomte, J. T. J., & La Mar, G. N. (1985) *J. Magn. Reson. 64*, 521−526.
van Gunsteren, W. F., & Berendsen, H. J. C. (1977) *Mol. Phys. 34*, 1311−1327.
Vyas, K., Rajarathnam, K., Lu, L. P., Emerson, S. D., La Mar, G. N., Krishnamoorthi, R., & Mizukami, H. (1993) *J. Biol. Chem. 268*, 14826−14835.
Wand, A. J., Di Stefano, D. L., Feng, Y., Roder, H., & Englander, S. W. (1989) *Biochemistry 28*, 186−194.
Weiner, S. J., Kollman, P. A., Nguyen, D. T., & Case, D. A. (1986) *J. Comput. Chem. 7*, 287−303.
Wüthrich, K. (1986) *NMR of Proteins and Nucleic Acids*, Wiley, New York.
Wüthrich, K. (1989) *Acc. Chem. Res. 22*, 36−44.

BI9507894